Computer Physics Communications 80 (1994) 259–273
North-Holland

Computer Physics Communications

keV particle bombardment of solids: molecular dynamics simulations and beyond

Dan N. Bernardo [1], Reena Bhatia and Barbara J. Garrison
Department of Chemistry, The Pennsylvania State University, University Park, PA 16802, USA

The bombardment of solids with keV atoms or ions leads to rather violent collisions with subsequent ejection of target particles. This review discusses computational aspects of molecular dynamics simulations designed to describe this process, and presents studies in which the calculations have played an important role in understanding the details of the bombardment and ejection processes at the atomic level. The molecular dynamics simulations in conjunction with comparable experiments allow this process to be used as a measure of surface structure. Recently experiments were performed that measured the energy and angular distributions of particles ejected in two electronic states. We have accordingly incorporated a simple electronic excitation/de-excitation model into the simulation and shown that collisional events are important to describe the measured distributions.

1. Introduction

The deposition of energy in a solid via keV particle bombardment leads to a complex sequence of atomic collisions and electronic excitations or ionization, with subsequent ejection of some particles from the target as shown in fig. 1. This process takes place in environments as diverse as the icy surfaces of interstellar bodies which are subject to high energy particles [1,2] and the faces of semiconductor chips during their analysis [3]. The latter process is often performed in the laboratory using ions as bombarding particles, and the ejected atoms and ions are analyzed with mass spectrometers.

The kinds of ejected particles (and the angles and velocities with which they are ejected) provide clues to the processes responsible for their production as well as the structure and composition of the target. The nature of the ejected particles is oftentimes known, and it becomes the researcher's task to deduce the original structure of the surface under study.

Theories have been suggested to provide means for linking the surface structure to the distributions of the various ejected particles. Consider, for example, the simplest case of particle ejection from a single crystal surface. It has been known for over three decades that the angular distributions of ejected particles show characteristic anisotropies corresponding to preferred ejections along certain crystallographic direction [4]. Two models have been proposed to explain the underlying mechanism of ejection. The first is the focusing collision theory [5], which assumes that the inherent crystalline order brings about a correlation between the successive collisions. This, in turn, leads to a preferential propagation of energy along close-packed rows of atoms and thus enhanced particle ejection in such directions. Second is the Lehmann–Sigmund mechanism,

Correspondence to: B.J. Garrison, Department of Chemistry, The Pennsylvania State University, University Park, PA 16802, USA.
[1] Department of Chemistry, P.O. Box 939, Rutgers University, Piscataway, NJ 08855, USA.

SSDI 0010-4655(93)E0108-Y

which employs the structure of the surface to explain the ejection pattern [6]. However, due to their neglect of the full three-dimensional structure of the crystal and their use of oversimplified assumptions, these models can only provide a qualitative account of the observed phenomena.

Computer simulations of the ejection event provide a way of eliminating many of the above assumptions and can offer a detailed picture of the mechanisms leading to the angular anisotropies. This approach, in turn, falls into two groups. One is the binary collision approximation, where the particle trajectory is taken as a sequence of two-body collisions [7–9]. The second involves molecular dynamics (MD) calculations, where simultaneous interactions of atoms in the model crystal are taken into consideration [10–14].

This review will focus on the study of the ejection process using MD simulation. In particular, this paper will show that (a) MD simulations can be used to account for the velocity and angular distributions of ejected atoms, (b) this method can also be used to deduce the most likely structure or arrangement of adsorbate systems, (c) incorporation of suitable electronic excitation models into the MD simulations allows one to examine the production of excited atoms during the ejection process and (d) for suitably identified events a simple model can be devised so as to obtain better statistics for comparison to the experiment. The system of choice is Rh metal as several experiments that measure the energy and angular distributions of neutral atoms ejected from these surfaces have been made [14,15].

2. Simulating the motion of atoms in the solid

In this section we discuss the method for simulating atomic collisions in a solid. The particular systems of interest involve heavy atoms (larger than 15 amu) moving at slow velocities (usually less than 20 000 m/s), and thus classical dynamics can be used to describe the atomic motions. A typical bombardment event ("trajectory") begins with a target crystal composed of several hundred atoms and a high-velocity bombarding particle which is aimed at the crystal (fig. 1). In these calculations the primary particles are Ar^+ ions as experimentally Ar is inexpensive and does not chemically react with the substrate. The Ar^+ ions are aimed perpendicular to the crystal with 1–5 keV in these simulations. The calculation of atomic motions then proceeds in two steps. First, a potential is used for calculating the forces between atoms. Second, Hamilton's equations of motion are integrated over some interval of time to predict the resulting position of each atom in the system. The integration is continued until the energy of each atom remaining in the solid drops below some value where it is highly unlikely that it will subsequently eject. At this point some atoms have been ejected and are above the crystal.

The simulation involves several conditions which are not commonly used in molecular dynamics studies of other systems (e.g. simulations of liquids, proteins). First, no periodic boundary conditions are used. This allows any energy from the energetic bombarding particle to be dissipated through the sides and bottom of the crystal, rather than unrealistically confining this excess energy to the target. Periodic boundary conditions would also force the system under study to correspond to a dense, correlated and periodic array of bombardment and ejection events on the surface. This is not the case in current experiments, which use very low dosages of bombarding particles to produce single, independent bombardment events. Second, no temperature constraints are imposed on the system since the bombardment process leads to a system that is not in equilibrium. Third, low-frequency vibrations in the crystal are neglected since the simulations are over in ~ 0.5 picosecond, a time shorter than many vibrational motions. Finally, the crystal size is chosen so that most of the ejection events are well described.

Choosing the algorithm for integrating the equations of motion is a computationally interesting problem, and is affected largely by the time dependence of the interatomic forces. It is assumed that for a given timestep the forces on the atoms are constant, i.e., the atoms do not experience large displacements from their original posi-

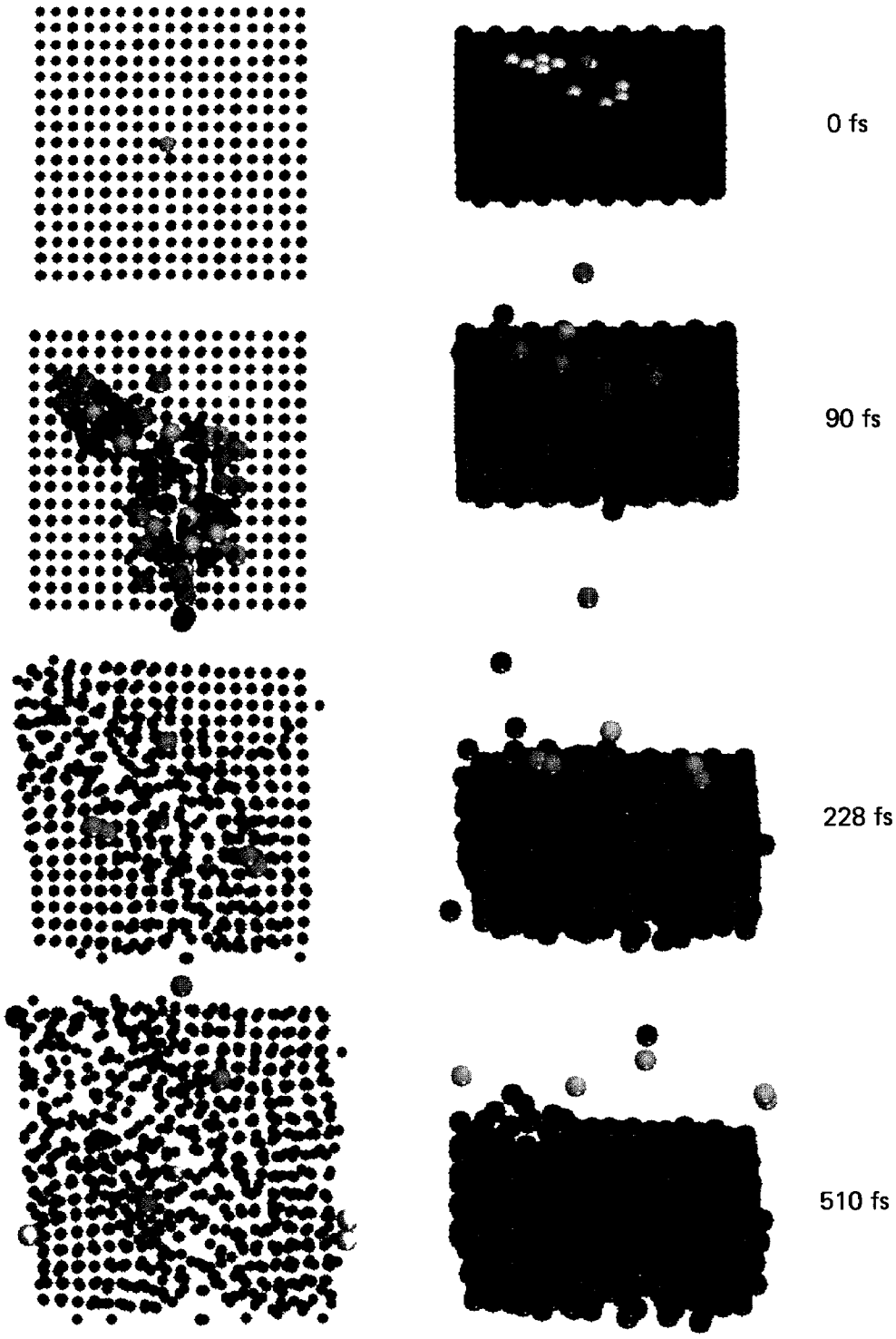

Fig. 1. Molecular dynamics simulation of a selected trajectory for ion-bombarded Rh{100}. Four stages of the simulation are shown. The frames on the left show a view of the crystal from the top. Atoms in the ground state are depicted as small blue spheres. Excited atoms are shown as larger spheres, with the color corresponding to the excitation probability. The colors, in order of increasing probability, are green, yellow, orange, red and white. (Blends of various colors are also used.) The bombarding particle is shown as a small gray sphere. The frames on the right show a side view of the same crystal, with atoms in the ground state also shown as large spheres. The yellow spheres in the uppermost frame denote atoms which are ejected at the end of the trajectory. The numbers at the right give the time during the collision cascade in fs where 1 fs = 10^{-15} second.

tions over a given timestep. These displacements are in turn dependent on the velocities. The simulation starts off with a high-velocity bombarding particle and ends with the ejection of several low-velocity atoms. This means that the atomic displacements during a timestep tend to be large at the start of the simulation and become smaller (by a factor of 3 or more) at the end of the simulation. In order to satisfy the constant-force (or small displacement) approximation it is computationally more efficient to use a variable-timestep integrator which would use small timesteps at the beginning of the simulation and gradually increase the timestep size as the calculation progresses [16]. The issue of computational efficiency is also complicated by the fact that interatomic potentials currently in use have varying degrees of complexity. Some potentials are easier to evaluate than others, and the development and accuracy of these potentials will be discussed in the following section.

Pairwise additive potentials have been utilized in computer simulations of the bombardment event since the early 1960s [17]. The parameters in the pair potential are fit to bulk properties such as cohesive energy, lattice constant and bulk modulus. For example, pairwise potentials were used in early simulations of the ion bombardment of Rh{111} [14]. The energy and angular distributions predicted by the simulations were in qualitative agreement with the experimental distributions. However, the positions of the maxima in the theoretical and experimental angular distributions differed by as much as 15°. Moreover, the calculated energy distributions are narrower and their maxima have lower values of the energy than the corresponding experimental distributions. The successes and failings of pair potentials can be explained quite simply. The pair potential description works because much of the trajectory is dominated by high-energy collisions which sample the repulsive wall, that is, the presence of an atom nearby. This is why, for example, angular distributions from all fcc{111} crystals look qualitatively similar. However, pair potentials start failing when the more chemical portion of the potential is important. Pair potentials cannot simultaneously describe the bulk binding environment (12 nearest neighbors for a fcc metal), the surface region (8 or 9 neighbors) and a gas phase dimer that has ejected. Peak positions in distributions are more influenced by the chemical or bonding portion. Thus a better description is needed.

The development of many-body potentials for large ensembles of atoms has boomed over the past few years. Investigators have sought to find systems and scattering regimes where these types of potential functions may be expressed in a mathematically tractable form. One such process is the ejection of atoms due to keV particle bombardment. This process is particularly attractive since numerous experiments on various systems have been carried out over the past few decades. This means that experimentally verifiable velocity and angular distributions of ejected atoms can be obtained from simulations as a means of testing the validity and accuracy of an interatomic potential function.

Since an atom ejected from the solid undergoes a rapid change in environment from the solid to the gas phase, one might expect a many-body potential which takes the atomic environment into account to be a better descriptor of the system. Such a many-body potential has been developed for the transition metals, and is derived from the embedded-atom method (EAM) of Daw and Baskes [18,19]. The EAM potential utilizes an ion-core representation of the metal atom embedded into the surrounding electron sea [20]. The energy for the ith atom is given by

$$E_i = F\left[\rho_i = \sum_{j \neq i} \rho_{\text{atomic}}(r_{ij})\right] + \tfrac{1}{2} \sum_{j \neq i} \phi(r_{ij}), \qquad (1)$$

where r_{ij} is the distance between the ith atom and the jth atom. The first term is the embedding function, which is the energy of the interaction of the ion core with the electron sea of density ρ_i. The embedding function is characteristic of a particular atom type and is assumed not to depend on the source of the electron density. Thus the embedding function for Rh is transferrable from one environment to the other if the electron density is known. For convenience, this density is assumed to be the instantaneous sum of

the atomic electron densities of the other atoms at the position of the atom of interest. Since these densities depend only on the distance between the atoms, forces are easily extracted for MD simulations. The second term is short-ranged and is the ion-core repulsion at a distance of separation r_{ij} of the two cores. Fitting procedures are described in refs. [20,21]. Parameters in the EAM potentials are fit to bulk properties including cohesive energy, lattice constant, elastic constants, vacancy formation energy and in our case the angular distributions of the keV particle bombardment process. As will be discussed in section 3, we can use this EAM density as a measure of the electronic environment.

2.1. Clean Rh{111}

Several EAM potentials were used in MD simulations of the ion bombardment of Rh{111}, the surface of which is shown in fig. 2. All fits improved the predicted energy distribution but there were varying degrees of agreement with the polar angular distributions [21]. The resulting energy and angular distributions (fig. 3) are more realistic than those obtained using pairwise potentials. The most dramatic difference observed between the pair potential and the EAM potential is in the predicted angle-integrated energy distributions. As shown in fig. 3, the distributions from experiment and calculations using the EAM potential are in excellent agreement while the calculated distribution using pair potentials is significantly different. (Remember the destructive nature of this process!) The peaks in the polar angle distributions as calculated using the EAM potential are shown in fig. 4 and are found to increase by about 10° from those predicted by the pair potentials. It is important to note that the azimuthal anisotropies (i.e., the ratio of the intensities in the $\phi = -30°$, $\phi = +30°$ and 0° directions) are well described by the pair potentials. In addition, the intensity in the normal direction increases relative to the intensity at $\theta = 40°$ as the ejected atom's kinetic energy increases in both the experimental and pair potential distributions.

The simulations can be used to explain the various anisotropies present in the angular distributions. For example, the largest peak at ($\theta = 40°$, $\phi = -30°$) has a contribution where a second layer atom moves upward at an angle and collides with a neighboring first layer atom, ejecting it. No such mechanism exists for ejection in the other azimuthal directions, and thus the peaks at ($\theta = 40°$) for both the $\phi = 0°$ and $\phi = 30°$ azimuths are considerably smaller. The many-body potential is noticeably better than the pair potential at describing the low-energy, grazing-angle (large θ) ejections. This suggests that this potential provides a more realistic description of the surface binding energy.

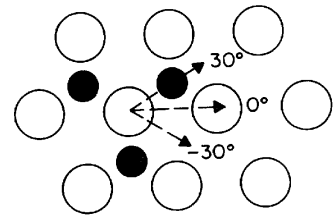

Fig. 2. Rh{111} crystal face. The open circles are first-layer atoms and the solid circles represent second-layer atoms. The azimuthal directions of $\phi = -30°$, 0° and 30° are shown.

Pair potentials have several other shortcomings which preclude their use in the study of certain solid-state systems. For example, the functions have no angular dependence, resulting in equilibrium crystal structures which are close packed. In other words, pairwise additive potentials cannot be used to describe open crystal

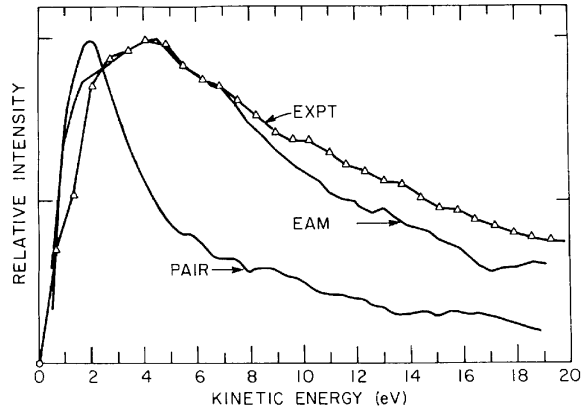

Fig. 3. Experimental and calculated kinetic energy distributions collected over all angles. In all cases the curves are peak normalized.

structures such as diamondlike lattices. In addition, these potentials do not take into consideration the changes in an atom's environment. The binding energy between two atoms, for instance, is independent of the number of atoms that surround these two.

It is these shortcomings in the pairwise potentials that have motivated the increasing use of many-body potentials in simulations [14]. It has been shown [21] that the use of pairwise additive potentials in MD simulations of the particle bombardment process results in energy distributions whose maxima are lower than the experimentally obtained distributions by a few eV. Use of a many-body potential results in an energy distribution whose maximum is much closer to that of the experiment. In this section we have examined the usefulness of the EAM potential in simulations involving the Rh{111} surface. Since the parameters of the potential are supposed to be applicable to any arbitrary configuration of Rh atoms, the same potential should be useful in simulations involving other crystal faces of Rh. This will be examined in the next section.

2.2. *Rh{331}*

The Rh{331} surface provides the first test case for using the many-body potential to predict energy and angular distributions. It is a stepped structure in which a third of the surface atoms are less coordinated than in Rh{111}, and in which another third are more coordinated, as shown in fig. 5. The step edges lower the symmetry of the surface (relative to Rh{111}), and the electron density distribution obtained from superposition of the atomic distributions is also considerably different for the two surfaces. To understand the effectiveness of the EAM potential, experimental and theoretical studies of ion-induced ejection from the Rh{331} surface [22] were undertaken. For the simulations, the same model potential used was as for Rh{111}.

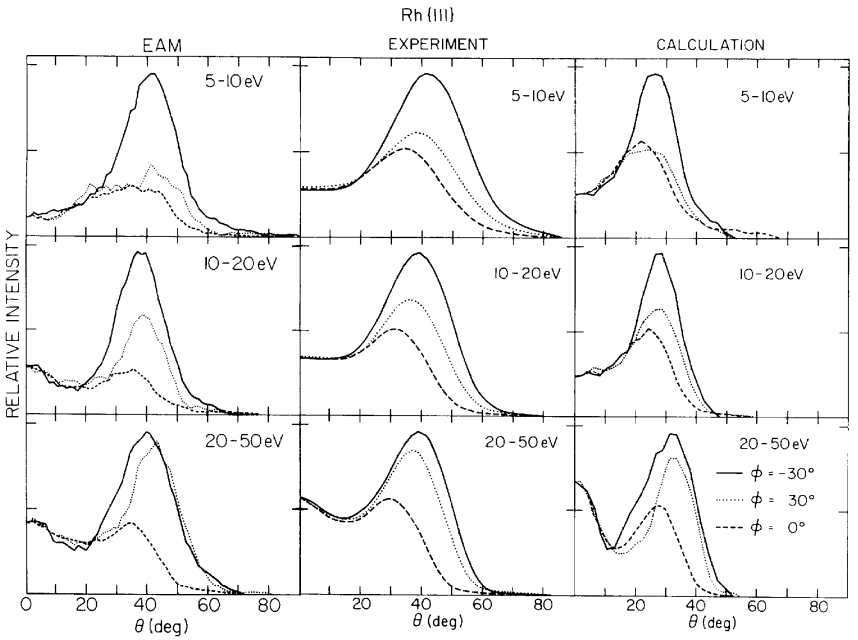

Fig. 4. Polar angle distributions for various azimuthal angles for fixed secondary kinetic energy of the Rh atoms. In each frame the data are normalized to the $\phi = -30°$ peak intensity. For the calculated data the full width at half maximum (FWHM) of the resolution is 15° in the polar angle. A constant solid angle is used in the histogramming procedure. The experimental-resolution is approximately the same. The surface normal corresponds to $\theta = 0°$. The right panel is labeled "calculation" and contains the pair potentials results.

Polar angle distributions of Rh atoms desorbed from an Ar-ion bombarded Rh{331} surface are presented in fig. 6a. These data are integrated in the kinetic energy range 10–20 eV. It is seen that ejection is strongly peaked at $\theta = 15°$ along the $\phi = 90°$ azimuth. It is also seen that the $\phi = -30°$ and $\phi = -90°$ azimuths have small but noticeable features at $\theta = 50°$–$60°$. Along the $\theta = 0°$ azimuth of Rh{331}, a small feature is observed at about $\theta = 40°$. The EAM potential, previously optimized for the flat Rh{111} surface, also accounts for the Rh{331} data, despite the different coordination of surface atoms between the two cases (fig. 6b). Still another, more "open" surface is the Rh{100} face, and it shall be shown that the same potential can be used in simulations involving that surface, too.

The experimental [23] polar angle (θ) distributions of Rh atoms desorbed from the Rh{100} surface along the $\phi = 0°$ (open) and $\phi = 45°$ (closed) azimuthal directions are shown in fig. 7. The off-normal intensity of the 0° azimuth is

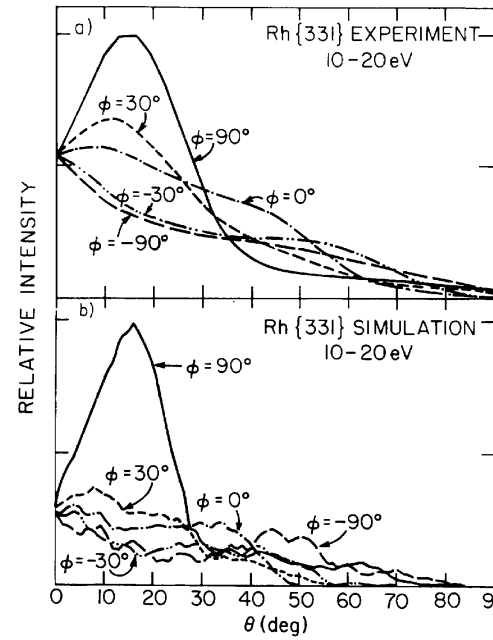

Fig. 6. Polar angle Rh atom distributions of keV ion-induced desorption from Rh single crystals. The 10–20 eV kinetic energy range is shown. (a) Rh{331}, experimental data; (b) Rh{331}, calculated curves employing the EAM.

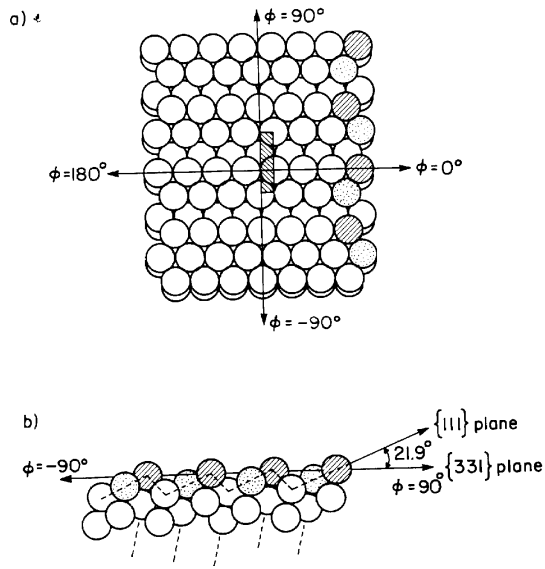

Fig. 5. (a) Rh{331} surface indication the definition of azimuths used in the text. The impact zone used in the classical dynamical simulation is shown at the center of the crystallite as a shaded box. (b) Rh{331} surface viewed from the $\phi = 0°$ direction. The shaded atoms correspond to the shaded atoms in (a). The dotted near-vertical lines indicate a major channeling direction.

higher than for the 45° direction, indicating that there is a strong preference for ejection along the open channels of the crystal, a behavior previously observed for Rh{111} [24]. In addition, ejection is focused into a polar angle of about 50° along the open direction and 35° for the close-packed direction.

The results of the classical molecular dynamics simulation of the desorption process are presented in fig. 7. As can be seen, the measured angular anisotropies are well reproduced by the calculation in the high-kinetic-energy regime. However, the agreement is less satisfactory in the low-energy range ($\lesssim 10$ eV). At present, the reason for this discrepancy is not clear. In any event, the main peaks in the azimuthal distributions are well-reproduced.

A "beam" of atoms escaping along any particular direction (such as $\theta = 50°$, $\phi = 0°$ for the Rh{100} face) can be used as a probe for locating adsorbates which bind in particular areas of the crystal face. Attenuation of the peak, for example, may indicate that an adsorbed atom is block-

ing ejection along a specific directions. In the following section, we shall describe the use of such a technique to study the adsorption of oxygen on Rh{111}.

2.3. O / Rh{111} – prediction of surface structure

The presence of adsorbates complicates simulation of the ejection process in several ways. First, additional potentials are required to describe the interactions between an adsorbed particle and the substrate as well as interactions among adsorbed particles. Second, introduction of an adsorbate may lower the symmetry of the system and complicate the energy and angular distributions of ejected target particles. Finally, the positions of the adsorbed particles may be unknown.

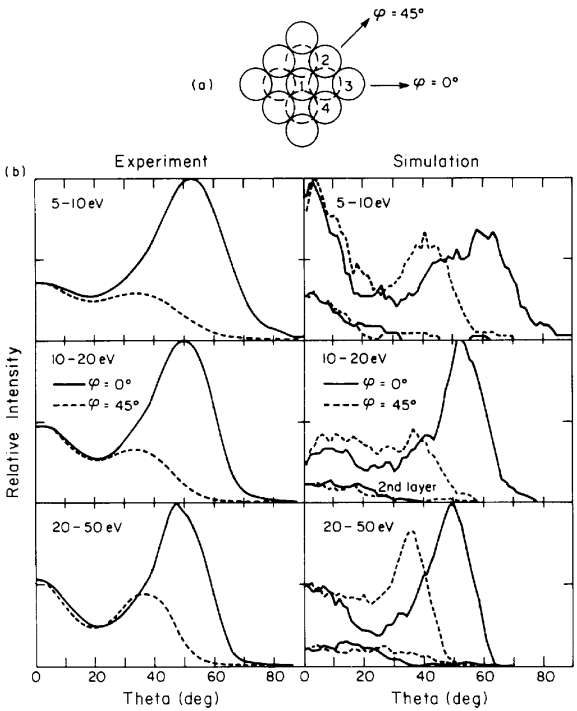

Fig. 7. (a) Rh{100} crystal face with $\phi = 0°$ (open) and $\phi = 45°$ (closed) azimuthal directions shown. The dashed circles denote the positions of the second layer atoms. (b) Experimental (right) and calculated (left) polar angle distributions for Rh atoms desorbed from Rh{100}. Solid lines correspond to ejection along $\phi = 0°$ and the dashed lines along the 45° direction for 5–10 eV (top), 10–20 eV (middle) and 20–50 eV (bottom) energy ranges of the ejected Rh atoms. The curves marked "2nd layer" are the distributions obtained by only collecting the second-layer atoms.

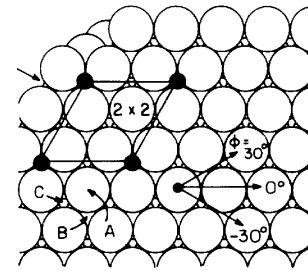

Fig. 8. The structure of the Rh{111} lattice and possible oxygen atom overlayer superstructures. Definition of the azimuthal angles, view of three high-symmetry atomic adsorbate sites and view of the p(2×2) super-structure.

Simulations provide a means of determining the most likely structures of adsorbate systems. Such a system can be subjected to experiments wherein the velocity and angular distributions of the ejected substrate atoms are determined. Simulations can then be run on several candidate structures. Comparison of the theoretically predicted distributions with their experimental counterparts then determines which of the candidate structures is most plausible.

The ordering and coverage of oxygen overlayers on Rh crystals have been extensively examined. The adsorption of oxygen on Rh{111} is of particular interest to us since earlier simulations on clean Rh{111} [21] allow comparison of the velocity and angular distributions of ejected Rh atoms from both clean and oxygen-covered surfaces. Oxygen may bind to several places on the {111} surface, and three of these high-symmetry sites are shown in fig. 8. The atop site is referred to as the A site, the threefold hollow over a second layer Rh atom is referred to as the B site, and the threefold hollow over a third layer Rh atom is referred to as the C site. A dynamical LEED study of the system indicates that the oxygen forms a p(2 × 2) overlayer with the atoms in the C site [25]. However, other evidence suggests that other arrangements are possible [26], and so the precise geometry of the O/Rh{111} system is not yet established.

In order to deduce the binding site of oxygen, experimental data for atoms ejected from clean [14,21] and oxygen-exposed [22] Rh{111} were first obtained. These data are presented in fig. 9 as polar angle distributions. The data from oxygen-covered Rh{111} exhibit distinct differences when compared to those obtained from clean Rh{111}. First, the intensity of Rh atom ejection is reduced by the presence of the oxygen overlayer, especially in the off-normal direction. Second, ejection along the $\phi = -30°$ azimuth is reduced more than ejection along the $\phi = +30°$ azimuth. Third, the polar angle at which off-normal ejection maximizes is 2°–10° closer to the surface normal

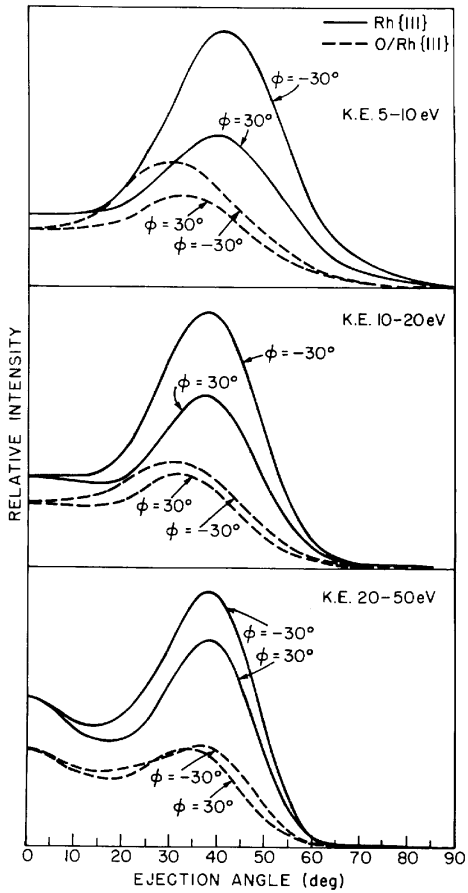

Fig. 9. Experimental polar angular distributions of Rh atoms ejected from clean and oxygen-covered Rh{111}. A polar angle of $\theta = 0°$ corresponds to normal ejection from the sample surface. The oxygen coverage displays an apparent p(2×2) LEED pattern.

compared to the data from clean Rh{111}. Could the above experimental findings be predicted in the simulations? Molecular dynamics simulations were first performed on ejection from both clean Rh{111} and from the p(2×2) O/Rh{111} system. Calculations for all three adsorption sites showed that for this system, the change in ejection yield with oxygen coverage was very small. This was in marked contrast to the experimental results, where the difference in yield is about a factor of 2 between the clean and oxygen covered surface.

Simulations involving ejection from the p(2×1) O/Rh{111} system were done next, and the results are shown in fig. 10. If oxygen atoms are assumed to bind in the A sites, the ejection signals along the $\phi = \pm 30°$ azimuths are reduced to about the same size. If oxygen atoms are assumed to bind in the B sites, then the signal is clearly more reduced along the $\phi = 30°$ azimuth than along the $\phi = -30°$ azimuth, especially for KE larger than 10 eV. This trend is opposite to what is observed in the data, which show preferential reduction of signal measured along the $\phi = -30°$ azimuthal direction upon oxygen adsorption. Finally, if the oxygen atoms are assumed to bind in the C sites, then for all KE ranges there is a larger reduction in the signal along the $\phi = -30°$ azimuth. The amount of signal reduction is similar to that observed in the experiments. Thus, the assumption of the C site in the p(2×1) O/Rh{111} system leads to good agreement between calculate ejection distributions and data in the KE range above 10 eV. It is seen that detailed classical dynamics calculations confirm the tentative conclusion that oxygen atoms bind in the C site and affect the Rh atom ejection distributions through directionally preferential blocking.

3. Simulating electronic excitations

There exist several methods for the calculation of electronic excitations. The choice of a method that is to be incorporated into molecular dynamics simulations is influenced by several scientific and computational requirements. For example,

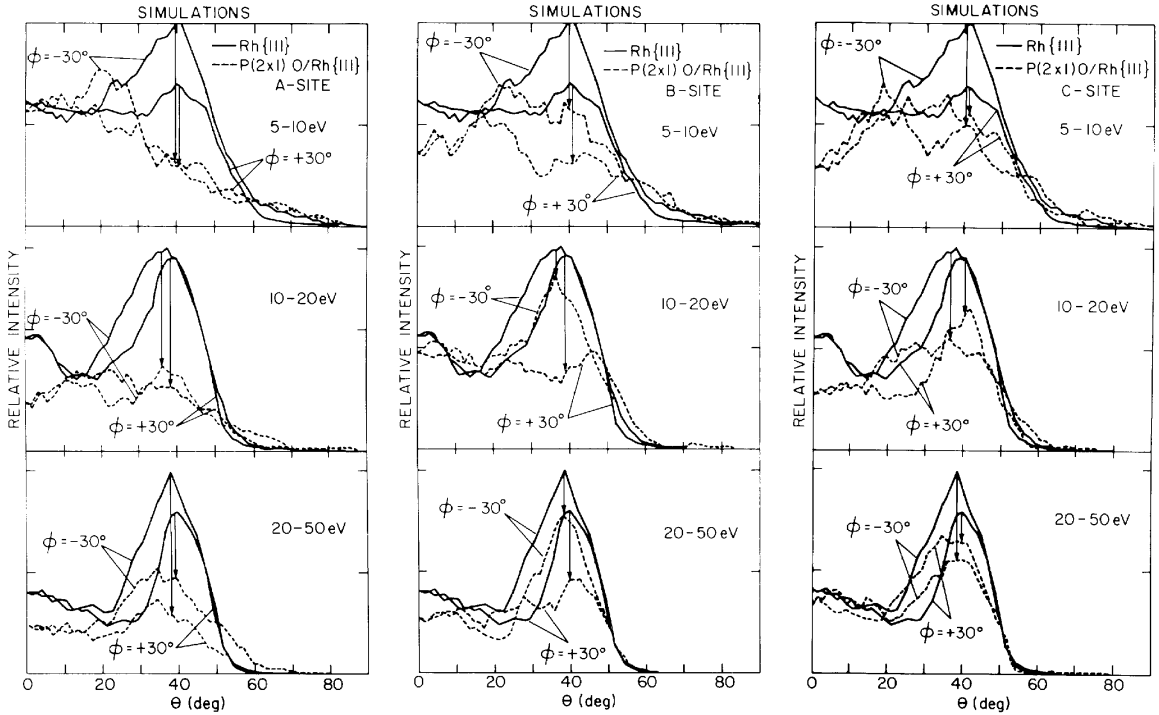

Fig. 10. Simulated polar angular distributions of Rh atoms ejected from clean Rh{111} and p(2×1) O/Rh{111} as a function of the energy of the ejected Rh atoms and the site of the adsorbed O atom....

elaborate excitation models which rely on electronic structure calculations are much slower than the accompanying molecular dynamics calculations and would defeat the computational efficiency that is one of the main advantages of the latter method.

Previous studies on the calculations of electronic excitations [27,28] have instead employed the collisional excitation model, which is computationally attractive since it requires no explicit electronic structure calculations. This model is based on the curve-crossing theory of Fano and Lichten [29] and assumes that colliding atoms are excited (with initial excitation probability P_0) when the interatomic distance drops below some threshold value. Once the collision is over, an atom's excitation is subjected to the time-dependent decay

$$\mathrm{d}P/\mathrm{d}t = -P/\tau. \tag{2}$$

The lifetime τ is based on some empirically determined, environment-sensitive quantity. It is assumed that relaxation is a result of the coupling between the excited electron and the electrons in the solid. In our more recent studies [30], τ is defined in terms of the electron density obtained from the EAM potential

$$1/\tau = c\rho_i, \tag{3}$$

where c is some constant and ρ_i is the same quantity as in eq. (1). This expression lets τ fluctuate about some constant value in the bulk and allows τ to approach infinity when the atom is far from the solid. This latter condition is necessary since current studies deal with metastable excited states.

The parametrization of the lifetime does not involve any assumptions regarding the velocity or angles of ejection. The assumption of a constant value of the exit velocity perpendicular to the surface, $v_\perp$, over the ejection trajectory has been used in previous studies to obtain a simple relation for the value of the final excitation probability. If an atom is excited at $z = 0$ Å and subse-

quently ejects with a constant $v_\perp$, then the final excitation probability is

$$P = P_0 \exp(-A/av_\perp), \quad (4)$$

where A/a is the decay coefficient [31]. This linear relation between $\log(P)$ and $1/v_\perp$ has been observed in numerous studies, although deviations from this relation have been found at low ejection velocities and have been attributed to binding energy effects [32–35]. The above relation will again be tested using the procedures outlined in this section.

The prediction of excited state populations proceeds as follows. In this section we present extensive velocity-resolved angular distributions of Rh atoms ejected from Rh{100} in the ground state, $^4F_{9/2}$, and the next higher-lying excited state, $^4F_{7/2}$, which has an excitation energy of 0.2 eV. We show that a combination of the nonradiative deexcitation approach with realistic atomic trajectories predicts distributions which are in good agreement with experimental results. The use of molecular dynamics simulations reveals some collisional mechanisms which have not been apparent in simpler implementations of the nonradiative deexcitation model. For example, atomic collisions 1–20 Å above the surface are found to be important for excitations at low velocities.

Results of the theoretical predictions and experiments are presented in fig. 11. Both sets of data represent the ratio of the excited state population (N^*) to the ground state population (N). The linear relation between $\log(N^*/N)$ and $1/v_\perp$ is observed at high velocities. At low velocities N^*/N becomes independent of $v_\perp$. This abrupt leveling off cannot be attributed to the binding energy effect, which produces a more gentle change in curvature.

The same N^*/N vs. $1/v_\perp$ behavior is observed in the theoretical predictions. The results of the simulations are perhaps better understood if excitation probabilities of individual atoms are examined (fig. 11b). The large spread observed in the individual probabilities is due to the various trajectories that the atoms experience during the excitation process. Each atom has a different history of initial excitation and subsequent relaxation, resulting in different final excitation probabilities. At high velocities most of the points are scattered about an exponentially decaying excitation probability on $1/v_\perp$, giving rise to the linear relation between $\log(N^*/N)$ and $1/v_\perp$.

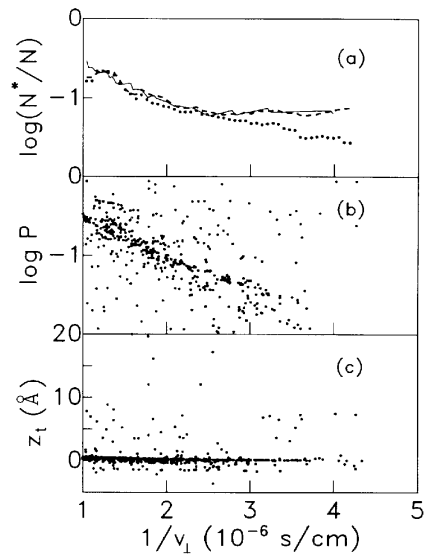

Fig. 11. Results of electronic excitation calculations. (a) Dashed line represents $\log(N^*/N)$ vs $1/v_\perp$ as predicted by simulations for particles ejected with $\theta < 20°$. Reevaluation of $\log(N^*/N)$ with the omission of atoms with $z_t > 1$ Å yields a result represented by the dotted line. The solid line represents the experimental result for atoms with $\theta < 10°$. (b) Excitation probabilities for individual atoms as predicted by the simulations. (c) Height at which an atom was last excited, z_t.

Insight into the low-velocity behavior of the excitation probability can be gained by again examining fig. 11b. As mentioned earlier, most of the excitation probabilities are exponentially decaying with $1/v_\perp$. However, there are ejected atoms whose excitation probabilities are quite high. The excitation history of these atoms can be examined using our molecular dynamics simulations, and in doing so, we find that these atoms have been last excited by collisions with other atoms some distance ($\sim$ 1–20 Å) above the surface (fig. 11c). One such collision is shown in fig. 1. Within the framework of the model, these atoms are far removed from interaction with the substrate, and thus their lifetimes are much longer. The enhanced excitation probability in

the low velocity regime arises from the atoms that are excited above the surface and simply do not decay or deexcite. Since slow moving atoms that are excited at the surface almost completely deexcite, the atoms excited above the surface contribute significantly to the total excitation probability in the low velocity region.

In this section it has been demonstrated that the collisional excitation approach is attractive from a computational as well as a scientific standpoint. It is sufficiently simple so as not to obscure the basic physics of the excitation event. It also allows the examination of excitations at the atomic level. When used in conjunction with molecular dynamics simulations, it allows examination of specific collision events and their role in producing atoms with unusually high (or low) final excitation probabilities.

4. Simulating collisions above the surface

The combination of a collisional excitation model with molecular dynamics simulations has led to the discovery of excitations above the surface as well as their important contribution to the average excitation probability at low ejection velocities. However, fig. 11c shows that relatively few of these collisions occur in a series of simulations. The majority of the collisions occur at or below the surface. In other words, the current application of molecular dynamics is relatively inefficient at simulating collisions above the surface. Thus the hope of explaining any angular dependence is slim. The development of a more efficient method shall be discussed in this section.

The simulation of atomic collisions a few Å above the surface involves first selecting two atoms and assigning them initial ejection angles, velocities and ejection times. The choice of ejection atoms and their ejection times is based on distributions obtained from prior molecular dynamics simulations. The probability $S(v, \theta, \phi)$ for ejection at a specific velocity and angle is based on the experimental distributions.

Two other assumptions are used. First, it is assumed that an atom is in its equilibrium position when it starts to leave the crystal. The displacement of atoms which are driven into the crystal and are later ejected at some other location on the surface are not taken into consideration. Second, it is assumed that clusters are not involved in collisions above the surface.

Once the initial velocities, angles, and ejections times of the two atoms are determined, the Rh dimer potential [21] from the same potential as used in the molecular dynamics simulation [36] is used to determine the distance of closest approach, r_c. If r_c is less than the threshold distance for excitation r_{th}, then the velocities and angles of the two atoms after the collision as well as the height z_t at which the collision occurs are calculated [37]. If the height is above some minimum value z_{to}, then both initial and final sets of velocities and angles are recorded.

The above procedure is iterated, each time for a new pair of ejecting atoms, until a sufficient number of collisions has occurred to allow the determination of $C(v, \theta, \phi)$, the velocity and angular distribution of atoms that have experienced a collision above the surface. The population of excited state atoms produced by collisions above the surface is given by

$$N_c^*(v, \theta, \phi) = C(v, \theta, \phi)\ P_0, \tag{5}$$

where P_0 is the initial value of the excitation probability as determined in ref. [38]. The corresponding population of atoms in the ground state is obtained using

$$N_c(v, \theta, \phi) = C(v, \theta, \phi)\ (1 - P_0). \tag{6}$$

In order to obtain the total populations of atoms in the excited and ground states, one must also include the contribution of atoms which are ejected and do not experience any collisions above the surface. The population of excited state atoms produced by collisions at the surface is given by

$$N_s^*(v, \theta, \phi) = S(v, \theta, \phi)\ P(v, \theta, \phi), \tag{7}$$

where $P(v, \theta, \phi)$ is the excitation probability for an atom ejected at the surface with velocity v, polar angle θ, and azimuthal angle ϕ. ($P(v, \theta, \phi)$ is fit with 2 parameters to the experimental data. This term does not involve the collisional model.)

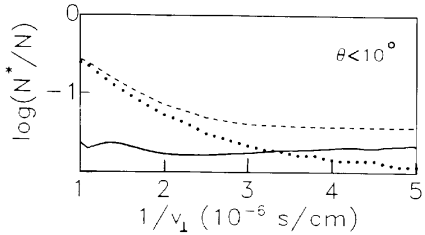

Fig. 12. Separation of N^*/N into its contributions from atoms excited at various heights. Theoretical predictions are for atoms ejected with energies from 10–20 eV. The solid line represents $\log(N_c^*/N)$, where N_c^* is the population of excited atoms produced by collisions a few angstrom above the surface. The dotted line represents $\log(N_s^*/N)$, where N_s^* is the population of excited atoms produced by collisions at the surface. The dashed line is the sum of the two contributions.

The corresponding population of ground state atoms is

$$N_s(v, \theta, \phi) = S(v, \theta, \phi)\,[1 - P(v, \theta, \phi)]. \quad (8)$$

The total populations of atoms in the excited and ground state are finally obtained by

$$N^*(v, \theta, \phi) = N_c^*(v, \theta, \phi) + N_s^*(v, \theta, \phi) \quad (9)$$

and

$$N(v, \theta, \phi) = N_c(v, \theta, \phi) + N_s(v, \theta, \phi). \quad (10)$$

Results of the simulation are shown in fig. 12. The ratio N^*/N clearly displays the same velocity dependence that is observed in the experiments. The real advantage of this set of simulations can be seen in the smoothness of the line describing N_c^*/N. The number of simulated collisions above the surface (30 000) was sufficient to allow determination of statistically significant values of N_c^*/N. This ratio remains fairly constant over the range of velocities under study. This indicates that collisional excitation can be thought of as a "background" process which occurs over all velocities. At low velocities it is the large contribution of N_c^* to N^* which leads to the leveling off of N^*/N at some constant value. Furthermore, the ratio N_s^*/N (which is the result of collisions at or below the surface) exhibits some curvature but does not level off. This means that if collisions at the surface were the only source of atomic excitations, the resulting N^*/N (which would then be equal to N_s^*/N) would not become constant at low velocities. This analysis clearly illustrates the importance of excited atoms produced by collisional excitation a few angstroms above the surface. It is the efficiency of the simulations procedure which allowed extraction of this information. These last two sections have thus illustrated the use of molecular dynamics simulations to model collisional processes in two very different spatial regions.

5. Present status, prospects, and conclusions

In this review, we have shown how molecular dynamics simulations can be used to understand many details of the particle bombardment process. Numerous target systems can now be modeled, and collisional and ejection processes understood at the atomic level. These simulations have been useful in studying the bombardment of clean metal surfaces and those with atomic overlayers.

The application of molecular dynamics simulations to more complex systems represents the next logical step in the development of this method. However, in the extension of this method one encounters several obstacles, both scientific and computational. Some of these problems are mentioned below.

Potentials for describing systems such as diamond lattices must describe the highly directional chemical bonding in these systems. The description of these complex interatomic forces leads to complicated potential functions [39–41], with concurrent increases in computational requirements. The development of heteroatomic potentials is yet another step in the quest to model increasingly complex systems, and is reflective of the movement from a simple, two-body view of the collision process to a many-body treatment that incorporates structural concepts found in both solid-state physics and chemistry.

The use of increasingly larger targets in simulations will, of course, lead to larger demands for computer memory. The size of a target is a function of the range of energies involved as well as

the periodicity of the surface. For example, a 1000-atom Rh target is reasonably sufficient to contain the collision cascade induced by a 3 keV bombarding Ar ion. There are several experimental techniques (e.g., secondary ion mass spectrometry using liquid metal ion sources) which involve much higher bombardment energies and larger collision cascades. Simulating these processes will require targets which are orders of magnitude larger than existing ones. The storage of atomic coordinates and velocities for these simulation may pose problems.

As demonstrated in this review, empirical models for describing electronic excitation can be coupled with molecular dynamics simulations to model the formation of excited species during the ejection event. More elaborate excitation models will be necessary to describe the production of multiple excitation states as well as the possibility of interstate crossings.

In summary, molecular dynamics simulations of the ion bombardment process is sufficiently developed to describe the ejection of particles from simple targets. The ability to examine collisions on the atomic level has led to the discovery of various mechanisms for the ejection and excitation of target atoms. The extension of this method to more complex systems awaits the development of suitable interatomic potentials and increases in computing resources.

Acknowledgements

We gratefully acknowledge the financial support of the National Science Foundation and the Office of Naval Research. We also appreciate collaborations with many experimentalists over the years.

References

[1] W.L. Brown and R.E. Johnson, Nucl. Instrum. Methods B 13 (1986) 295.
[2] D.W. Brenner and B.J. Garrison, Phys. Rev. B 34 (1986) 5782.
[3] R. Blumenthal, K.P. Caffey, E. Furman, B.J. Garrison and N. Winograd, Phys. Rev. B 44 (1991) 12830.
[4] G.K. Wehner, J. Appl. Phys. 26 (1955) 1056.
[5] R.H. Silsbee, J. Appl. Phys. 28 (1957) 1246.
[6] C. Lehmann and P. Sigmund, Phys. Status Solidi 16 (1966) 507.
[7] F.J. Smith, Physica 30 (1964) 497.
[8] H. O'Hara and F.J. Smith, J. Comput. Phys. 5 (1970) 328.
[9] M.T. Robinson and I.M. Torrens, Phys. Rev. B 9 (1974) 5008.
[10] D.E. Harrison, Jr., J.P. Johnson III and N.S. Levy, Appl. Phys. Lett. 8 (1966) 33.
[11] B.J. Garrison and N. Winograd, Science 216 (1982) 805.
[12] M.H. Shapiro, P.K. Haff, T.A. Tombrello, D.E. Harrison Jr. and R.P. Webb, Radiat. Eff. 89 (1985) 243.
[13] D.Y. Lo, M.H. Shapiro and T.A. Tombrello, Mater. Res. Soc. Symp. Proc. 174 (1987) 449.
[14] B.J. Garrison, N. Winograd, C.T. Reimann and D.E. Harrison Jr., Phys. Rev. B 36 (1987) 3516.
[15] J.P. Baxter, J. Singh, G.A. Schick, P.H. Kobrin and N. Winograd, Nucl. Instrum. Methods B 17 (1986) 300.
[16] D.E. Harrison, W.L. Gay and H.M. Effron, J. Math. Phys. 10 (1969) 1179.
[17] J.B. Gibson, A.N. Goland, M. Milgram and G.H. Vineyard, Phys. Rev. 120 (1960) 1229.
[18] M.S. Daw and M.I. Baskes, Phys. Rev. Lett 50 (1983) 1285.
[19] M.S. Daw and M.I. Baskes, Phys. Rev. B 29 (1984) 6443.
[20] S.M. Foiles, M.I. Baskes and M.S. Daw, Phys. Rev. B 33 (1986) 7983.
[21] B.J. Garrison, N. Winograd, D.M. Deaven, C.T. Reimann, D.Y. Lo, T.A. Tombrello, D.E. Harrison, Jr. and M.H. Shapiro, Phys. Rev. B 37 (1988) 7197.
[22] C.T. Reimann, K. Walzl, M. El-Maazawi, D.M. Deaven, B.J. Garrison and N. Winograd, J. Chem. Phys. 89 (1988) 2539.
[23] R. Maboudian, Z. Postawa, M. El-Maazawi, B.J. Garrison and N. Winograd, Phys. Rev. B 42 (1990) 7311.
[24] J. Singh, C.T. Reimann, J.P. Baxter, G.A. Schick, P.H. Kobrin, B.J. Garrison and N. Winograd, J. Vac. Sci. Technol. A 5 (1987) 1191.
[25] P.C. Wong, K.C. Hui, M.Y. Zhou and K.A.R. Mitchell, Surf. Sci. 165 (1986) L21.
[26] D.G. Castner and G.A. Somorjai, Appl. Surf. Sci. 6 (1990) 29.
[27] M.H. Shapiro and J. Fine, Nucl. Instrum. Methods B 44 (1989) 43.
[28] J.J. Vrakking and A. Kroes, Surf. Sci. 84 (1979) 153.
[29] U. Fano and W. Lichten, Phys. Rev. Lett. 14 (1965) 627.
[30] R. Bhatia and B.J. Garrison, unpublished results.
[31] H.D. Hagstrum, Phys. Rev. 96 (1954) 336.
[32] D. Grischkowsky, M.L. Yu and A.C. Balant, Surf. Sci. 127 (1983) 351.
[33] M.L. Yu and N.D. Lang, Phys. Rev. Lett. 50 (1983) 127.
[34] J.H. Lin and B.J. Garrison, J. Vac. Sci. Technol. A 1 (1983) 1205.
[35] B.J. Garrison, Surf. Sci. 167 (1986) L225.
[36] D.N. Bernardo, M. El-Maazawi, R. Maboudian, Z.

Postawa, N. Winograd and B.J. Garrison, J. Chem. Phys. 97 (1992) 3846.
[37] D.N. Bernardo and B.J. Garrison, J. Chem. Phys. 97 (1992) 6910.
[38] N. Winograd, M. El-Maazawi, R. Maboudian, Z. Postawa, D.N. Bernardo and B.J. Garrison, J. Chem. Phys. 96 (1992) 6314.
[39] J. Tersoff, Phys. Rev. Lett. 56 (1986) 632.
[40] F.H. Stillinger and T.A. Weber, Phys. Rev. B 31 (1985) 5262.
[41] D.W. Brenner, Phys. Rev. B 42 (1990) 9458.